

# Artificial Magnetic Materials Using Fractal Hilbert Curves

Leila Yousefi, *Member, IEEE*, and Omar M. Ramahi, *Fellow, IEEE*

**Abstract**—Novel configurations based on Fractal Hilbert curves are proposed for realizing artificial magnetic materials. It is shown that the proposed configuration gives significant rise to miniaturization of artificial unit cells which in turn results in higher homogeneity in the material, and reduction in the profile of the artificial substrate. Analytical formulas are proposed for design and optimization of the presented structures, and are verified through full wave numerical characterization. The electromagnetic properties of the proposed structures are studied in detail and compared to square spiral from the point of view of size reduction, maximum value of the resultant permeability, magnetic loss, and frequency dispersion. To validate the analytical model and the numerical simulation results, an artificial substrate containing second-order Fractal Hilbert curve is fabricated and experimentally characterized using a microstrip-based characterization method.

**Index Terms**—Artificial magnetic materials, Fractal Hilbert curves, metamaterials, microstrip-line based characterization, permeability.

## I. INTRODUCTION

WHEN exposed to an applied electromagnetic field, magneto-dielectric materials are polarized both electrically and magnetically, so they exhibit enhanced relative permeability and permittivity.

Recently it has been shown that utilizing magneto-dielectric materials instead of dielectrics with high permittivity offers many advantages in an important class of applications [1]–[8]. In [1], it was shown that using materials with high permeability for antenna miniaturization can increase the bandwidth while materials with high permittivity would shrink the bandwidth. Furthermore, when materials with only high permittivity are used for antenna miniaturization, the high impedance mismatch between the substrate and the air decreases the efficiency of the system, while in the case of using magneto-dielectric materials, the impedance mismatch is smaller leading to the higher efficiency for the miniaturized antenna. It was shown in [2] that magneto-dielectric resonator antennas have wider impedance bandwidth than dielectric resonator antennas. In [3], a meander

Manuscript received August 27, 2009; revised November 21, 2009; accepted February 01, 2010. Date of publication May 18, 2010; date of current version August 05, 2010. This work was supported by Research in Motion and the National Science and Engineering Research Council of Canada under the NSERC/RIM Industrial Research Chair Program and the NSERC Discovery Grant Program.

The authors are with the Electrical and Computer Engineering Department, University of Waterloo, Waterloo, ON N2L 3G1, Canada (e-mail: lyousefi@uwaterloo.ca; oramahi@ece.uwaterloo.ca).

Color versions of one or more of the figures in this paper are available online at <http://ieeexplore.ieee.org>.

Digital Object Identifier 10.1109/TAP.2010.2050438

line type antenna using a magneto-dielectric material as a substrate was proposed for using in RFID systems. In [4] magneto-dielectric materials were used as a superstrate to increase the gain of a patch antenna leading to lower profile in comparison to antennas with dielectric superstrates. In [7] magneto-dielectric materials were used as the substrate of a mushroom-type electromagnetic band gap structure (EBG). The results in [7] showed that using magneto-dielectrics could increase the in-phase reflection bandwidth of EBGs when they are used as artificial magnetic ground planes.

For low-loss applications in the microwave region, natural material choices are limited to nonmagnetic dielectrics. When requiring relatively high permeability, the choices are limited to ferrite composites which provide high levels of magnetic loss [9]–[12]. Therefore, artificial magnetic materials are designed to provide desirable permeability and permittivity with manageable loss at these frequencies [13]–[19]. In spite of double negative metamaterials which are designed to provide negative permeability and permittivity, the goal of designing artificial magnetic materials is to provide an enhanced positive value for permeability.

The idea of using the split-ring as an artificial magnetic particle was introduced first in [20]. The works on realizing such a media started in the late 1990's [13]–[15]. Since then, engineers have proposed numerous types of inclusions [16]–[19]. The single and coupled split ring resonators (SRR), modified ring resonators, paired ping resonators, metasolenoid [16], split square spiral configuration [18], are some of the most popular configurations used in previous works. Each proposed structure provides its own advantages and disadvantages in terms of resultant permeability and dissipation. For example, in [16] it was shown that the metasolenoid configuration provides higher permeability in comparison to SRR configurations, or using split square spiral configuration results in artificial magnetic materials with smaller unit cells when compared to SRR and metasolenoid [17], [18].

One of the most important applications of artificial magnetic materials is implementing miniaturized planar structures, specifically miniaturized microstrip antennas [18], [19], [21]–[24]. Although it was shown that by using these materials, significant miniaturization factors could be achieved in the planar sizes of the antennas, the height of the substrate is limited by the size of the unit cell of the artificial structures. The size of the developed artificial unit cells are typically much smaller than the wavelength (smaller than  $\lambda/20$ ), yet they yield a large antenna profile (for example, for a microstrip antenna operating at 200 MHz, the smallest profile achieved is 2 cm [18]). Therefore, miniaturizing the unit cell of artificial materials not only provides better homogeneity, but also decreases the antenna profile.

With the aim of further miniaturization, other sub-wavelength particles have been recently proposed such as spiral resonators [17], [18], capacitively loaded embedded-circuit particles [25]–[27], as well as lumped-element based metamaterials [28]. In [17], it was shown that using spiral resonators decreases the size of the inclusion by a factor of 2 when compared to SRRs (split ring resonators). In [25]–[27], using parallel-plate capacitors, inclusions as small as  $\lambda/27$  are developed. (Note that in this paper, by  $\lambda$  we mean the wavelength in the host dielectric at the resonance frequency. Since by using a high- $k$  dielectric, the size of the inclusion decreases, and therefore, it is not useful to compare different inclusions based on wavelength in the air.) However; the structures in [25]–[27] are three dimensional and cannot be realized using printed circuit board technology. Using lumped elements within the inclusions, unit cells as small as  $\lambda/52$  were developed in [28]. The solution proposed in [28] is promising, however, lumped elements need to be soldered into place for each unit cell which makes the fabrication process difficult and time-consuming. In [18], using square spirals unit cells as small as  $\lambda/32$  were developed and used for antenna miniaturization. The structure introduced in [17], can be realized by simple printed technology. In this paper, we introduce fractal curves as inclusions for artificial magnetic material to further increase the miniaturization potential.

Previous works on using fractal geometries in developing artificial structures included frequency selective surfaces [29], high-impedance surfaces [30]–[35], left-handed metamaterials [36], and complementary split-ring resonators [37]. An extended class of space-filling wire structures based on grid-graph Hamiltonian paths and cycles has also been investigated in [38].

In this work, the use of Fractal curves to miniaturize artificial magnetic materials is investigated. This idea was proposed for the first time as a conference paper in our previous work [39]. Combining the square spiral loop configuration with fractal Hilbert curves, a new configuration is proposed to realize further miniaturization for artificial particles. It is shown that by using fourth-order fractal Hilbert curves, inclusions as small as  $\lambda/73$  can be realized. Using higher order Hilbert curves results in even smaller unit cells. Analytical formulas for design and analysis of the proposed structures are presented. Full-wave numerical characterization and experimental testing is carried out to validate the analytical results. The electromagnetic behavior of the proposed structures are investigated from the point of view of size reduction, maximum value of the resultant permeability, magnetic loss, and frequency dispersion.

The organization of this paper is as follows: In Section II, the new inclusions based on fractal Hilbert curves are introduced and analyzed. Analytical formulas for design and analysis of the proposed structures are presented, and full-wave numerical characterization is performed to verify the analytical results. Furthermore, using the analytical model and numerical simulation results, the proposed inclusions are compared to spiral inclusions. In Section III, second-order Fractal Hilbert inclusions were fabricated and characterized. For experimental characterization, we have used a new method reported in our prior work [40]. Summary and conclusion are provided in Section IV.

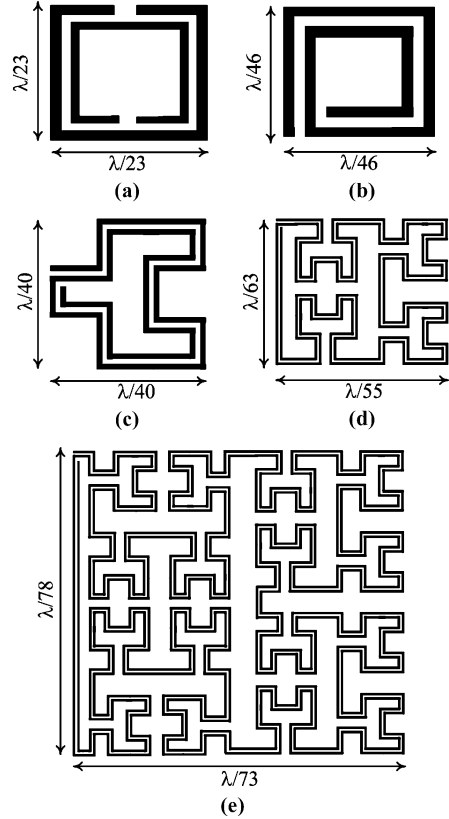


Fig. 1. (a) SRR. (b) Square spiral. (c) Second-order Fractal Hilbert inclusion. (d) Third-order Fractal Hilbert inclusion. (e) Fourth-order Fractal Hilbert inclusion. Note that as the order of Hilbert curve increases, the size of inclusion decreases.

## II. ARTIFICIAL MAGNETIC MATERIALS BASED ON FRACTAL HILBERT CURVES

Fig. 1 shows the proposed structures for metamaterial inclusions based on Hilbert curves, along with the split ring resonators (SRR) and spiral structures. Using circuit models, it was shown in [17] that the effective capacitance of the spiral configuration is four times of that of the SRR. Therefore, spirals can reduce the resonance frequency of the inclusion by a factor of 2. This claim was verified numerically and experimentally in [17]. The structures proposed in this work combine the idea of using spiral configuration (proposed in [17]) and Fractal Hilbert curve to provide inclusions with smaller size.

The dimensions of the inclusions as a fraction of the wavelength in the dielectric at the resonance frequency are shown in Fig. 1. Clearly observed is that when using a fourth-order Fractal Hilbert curve makes it possible to realize inclusion as small as  $0.014\lambda$ . This size is 63% of the size of spiral inclusion and 32% of the size of SRR.

### A. Analytical Model

Fig. 2 shows a unit cell of a third-order Hilbert inclusion. In what follows, a general formulation, which can be used for any order of Hilbert inclusions, is derived for the effective permeability. The unit cell in Fig. 2 has dimensions of  $\Delta x$ ,  $\Delta y$ , and  $\Delta z$  in the x, y, and z directions, respectively. An applied external magnetic field  $H_{ext}$  in the y direction induces an electromotive

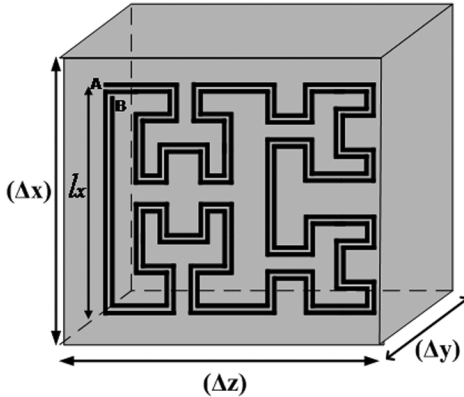


Fig. 2. A unit cell of engineered magnetic substrate composed of inclusions with 3rd order Hilbert Curve.

force emf in the ring. Applying Faraday's law, one can obtain the induced emf as

$$\begin{aligned} \text{emf} &= -j\omega\phi = -j\omega\mu_0S(H_{\text{ext}} + H_{\text{ind}}) \\ &= -j\omega\mu_0S\left(H_{\text{ext}} + 2\frac{I}{\Delta y}\right) \end{aligned} \quad (1)$$

where  $\omega$  is the frequency of the external field,  $H_{\text{ind}}$  is the induced magnetic field,  $I$  is the induced current, and  $S$  is the area enclosed by the inclusion. Since the dimensions of the unit cell in artificial materials are small in comparison to the wavelength, we assume a uniform magnetic field over the area of the unit cell.

The generated emf is related to the impedance of the rings and the induced current as

$$\text{emf} = Z_{\text{inc}}I \quad (2)$$

where  $Z_{\text{inc}}$  is the impedance of the metallic inclusion.

Equating (1) and (2) yields

$$-j\omega\mu_0SH_{\text{ext}} = \left(Z_{\text{inc}} + j\omega\frac{2S\mu_0}{\Delta y}\right)I. \quad (3)$$

From (3), it is observed that the effective inductance,  $L_{\text{eff}}$  of the inclusions can be defined as

$$L_{\text{eff}} = \frac{2S\mu_0}{\Delta y}. \quad (4)$$

The magnetic polarization,  $M$  defined as the average of the induced magnetic dipole moments can be expressed as

$$M = \lim_{\Delta v \rightarrow 0} \frac{1}{\Delta v} \sum_{i=1}^n m_i = \frac{2SI}{\Delta x \Delta y \Delta z}. \quad (5)$$

Using (3) and (5), the relative permeability  $\mu_r$  is obtained as

$$\mu_r = 1 - K \frac{j\omega L_{\text{eff}}}{Z_{\text{inc}} + j\omega L_{\text{eff}}}, \quad K = \frac{S}{\Delta x \Delta z}. \quad (6)$$

It should be noted that the substrate whose unit cell is shown in Fig. 2 can provide magnetic moment vectors only in the direction perpendicular to the inclusion surface (i.e., the effective permeability formulated in (6) represents the yy component of the permeability tensor). For x-directed and z-directed magnetic

fields, the effective permeability will be equal to that of the host media which is unity for nonmagnetic substrates. Therefore, the artificial substrate will be anisotropic with permeability tensor of

$$\mu = \mu_0 \begin{pmatrix} 1 & 0 & 0 \\ 0 & \mu_r & 0 \\ 0 & 0 & 1 \end{pmatrix}. \quad (7)$$

To achieve isotropic artificial substrates with the same effective permeability in all the three directions of x, y, and z, two inclusions with the surfaces perpendicular to the x, and z directions should be added to the unit cell shown in Fig. 2. If these two inclusions have the same structure as the inclusion perpendicular to the y direction, the same effective permeability formulated in (6) will be achieved in the x, and z directions.

The formula given in (6) is general and can be used for Hilbert inclusions of any order. The only difference between various orders would be in the value of the inclusion impedance,  $Z_{\text{inc}}$ , and the effective inductance,  $L_{\text{eff}}$ .

The effective inductance,  $L_{\text{eff}}$  given in (4) is a function of the area  $S$ , enclosed by the inclusion; and since this area varies by the order,  $n$ , of Fractal Hilbert curve, the effective inductance would be dependent on  $n$ .  $L_{\text{eff}}$  is given as

$$L_{\text{eff}} = \frac{2\mu_0}{\Delta y}S = \frac{2\mu_0}{\Delta y} \begin{cases} 6\left(\frac{l_x}{2^n-1}\right)^2 & n = 2 \\ l_x^2 \frac{2^n-2^{n-1}+1}{2^n-1} & n > 2 \end{cases} \quad (8)$$

where  $l_x$  is the dimension of the inclusion in the x direction (see Fig. 2). Equation (8) can be proved using mathematical induction principle [41].

The inclusion impedance,  $Z_{\text{inc}}$ , consists of two parts:  $R_{\text{eff}}$ , which models the ohmic loss of the metallic inclusions due to the finite conductivity of the strips, and the other part models the mutual impedance between external and internal loops,  $Z_{\text{mut}}$ .  $R_{\text{eff}}$ , can be calculated using the Ohm's law

$$R_{\text{eff}} = \frac{l_{\text{total}}}{\sigma(w\delta)}, \quad \delta = \sqrt{\frac{2}{\omega\mu_0\sigma}} \quad (9)$$

where  $\sigma$  and  $\delta$  are the conductivity and skin depth, respectively,  $w$  is the width of metallic strips and  $l_{\text{total}}$  is the total length of the metallic strips.  $l_{\text{total}}$  is given as

$$l_{\text{total}} = 2l_x \begin{cases} \frac{2^{2n}-2}{2^n-1} & n = 2 \\ \frac{2^{2n}+2^n}{2^n-1} & n > 2 \end{cases} \quad (10)$$

Equation (10) can be proved using mathematical induction principle [41]. In the proposed inclusions, the internal loop follows the shape of the external loop, therefore the mutual impedance between external and internal loops  $Z_{\text{mut}}$  can be modeled as the per-unit-length mutual impedance of the strips,  $Z_{\text{pul}}$ , times the average length of the strips,  $l_{\text{avg}}$

$$Z_{\text{mut}} = Z_{\text{pul}}l_{\text{avg}} \quad (11)$$

where

$$l_{\text{avg}} = (l_x - w - g/2) \begin{cases} \frac{2^{2n}-2}{2^n-1} & n = 2 \\ \frac{2^{2n}+2^n}{2^n-1} & n > 2 \end{cases} \quad (12)$$

and  $g$  is the gap between the metallic strips. The per-unit-length impedance,  $Z_{\text{pul}}$  is calculated using conformal mapping technique for the coplanar strip lines [42]

$$\begin{aligned} Z_{\text{pul}} &= \frac{1}{j\omega\epsilon_0\epsilon_r(1-j\tan\delta)} \frac{K(s)}{K(\sqrt{1-s^2})} \\ s &= \frac{g}{g+2w} \\ K(s) &= \int_0^{\frac{\pi}{2}} \frac{d\phi}{\sqrt{1-s^2\sin^2\phi}} \end{aligned} \quad (13)$$

where  $\epsilon_r$  and  $\tan\delta$  are the relative permittivity and the loss tangent of the host substrate, respectively. The impedance given in (13) contains a parallel combination of a capacitance,  $C_{\text{eff}}$  and a conductance,  $G_{\text{eff}}$  to model the capacitance between the metallic strips and the loss due to the conductivity of the host substrate.

It should be noted that this model considers the capacitance between two adjacent strips while it neglects the capacitance between non-adjacent strips. Therefore, the accuracy of this model increases when the space between non-adjacent strips is much larger than the space between adjacent strips. However, for the compact structures or for high order fractal curves, where the space between non-adjacent strips is comparable to the space between adjacent strips, this model gives only an approximation of the relative permeability that can be used to initiate a design. To extract exact relative permeability, one needs to use the full wave simulation method as explained below in Section II-B.

The proposed analytical formula developed in (6) fits the Lorentz model [43]

$$\mu_r = 1 + \frac{\omega_{pm}^2}{\omega_{0m}^2 - \omega^2 + jG_m\omega} \quad (14)$$

if the following substitutions are made:

$$\begin{aligned} \omega_{pm} &= \sqrt{K}\omega \\ \omega_{0m} &= \frac{1}{\sqrt{L_{\text{eff}}C_{\text{eff}}}} \\ G_m &= \frac{R_{\text{eff}}}{L_{\text{eff}}} \end{aligned} \quad (15)$$

Here, the  $\tan\delta$  term in (13) has been ignored since it is, for a typical host substrate, several orders of magnitude smaller than one.

The approach introduced in this section for deriving relative permeability of Hilbert inclusions can be used for square spirals too, and results in the same formula derived in (6). The only difference would be in the value of the effective lumped elements,  $L_{\text{eff}}$ ,  $C_{\text{eff}}$ , and  $Z_{\text{inc}}$ . Equation (16) illustrates the parameters that should be replaced so that (6) can be used for spiral inclusions.

$$\begin{aligned} S_{\text{spiral}} &= l_x^2 \\ l_{\text{avg,Spiral}} &= 4(l_x - w - g/2) \\ l_{\text{total,Spiral}} &= 8l_x. \end{aligned} \quad (16)$$

TABLE I  
COMPARISON OF THE FRACTAL SPIRAL INCLUSIONS WITH NON-FRACTAL SPIRAL INCLUSION

$n$	$L_{\text{eff}}$	$C_{\text{eff}}$	$R_{\text{eff}}$	Resonance Frequency
2	0.67	1.16	1.16	1.14
3	0.71	2.57	2.57	0.74
4	0.60	4.53	4.53	0.61
5	0.55	8.51	8.51	0.46
6	0.52	16.5	16.5	0.34

Using the above formulas, Table I compares the effective inductance, capacitance, resistance, and the resonance frequency of Hilbert inclusions with those parameters of the square spiral. The electrical parameters of the host substrate and the geometrical parameters of the unit cell and metallic strips are assumed to be the same for all the Hilbert inclusions and spiral.

From Table I, using Fractal Hilbert inclusions instead of square spirals reduces the effective inductance while increasing the effective capacitance in such a way that the resonance frequency would be smaller for Fractal Hilbert curves with  $n > 2$ . Therefore, using structures with Hilbert curves of order 3 or higher results in miniaturization of inclusions. We also observe that the miniaturization factor increases with the order of Hilbert curves.

Table I also gives higher value of effective resistance for Hilbert inclusions when compared to spirals. Increasing the effective resistance in the circuit model results in lower  $Q$  factor, which in turn results in lower rate of change in the resultant permeability with respect to frequency. Therefore, lower frequency dispersion can be achieved for the artificial medium. On the other hand, any increase in the effective resistance results in an increase in the magnetic loss of the artificial medium. Furthermore, since the effective inductance is reduced, it is expected that the maximum value of the relative permeability would be smaller for Hilbert inclusions when compared to spiral.

As a conclusion, the analytical models developed here predict that using Fractal Hilbert curves with order 3 or higher results in miniaturization of the inclusions, and, furthermore, in a reduction of the frequency dispersion of the artificial medium. The drawbacks would be lower resultant permeability and higher magnetic loss. This conclusion will be verified in part C using full wave numerical simulation.

### B. Numerical Full Wave Analysis

In order to verify the accuracy of the analytical model developed above, a full-wave numerical analysis setup is developed in this section to characterize the proposed engineered materials. The simulation setup is shown in Fig. 3.

In the simulation setup, periodic boundary conditions are used in the  $z$  and  $y$  directions around a unit cell to model an infinite slab, and perfect matched layers absorbing boundaries are used in the  $x$  direction to prevent reflections from the computational domain walls. For characterization, the well known plane wave analysis method is used [44]–[46]. In this method, the effective parameters,  $\mu_{\text{eff}}$  and  $\epsilon_{\text{eff}}$ , are extracted from the

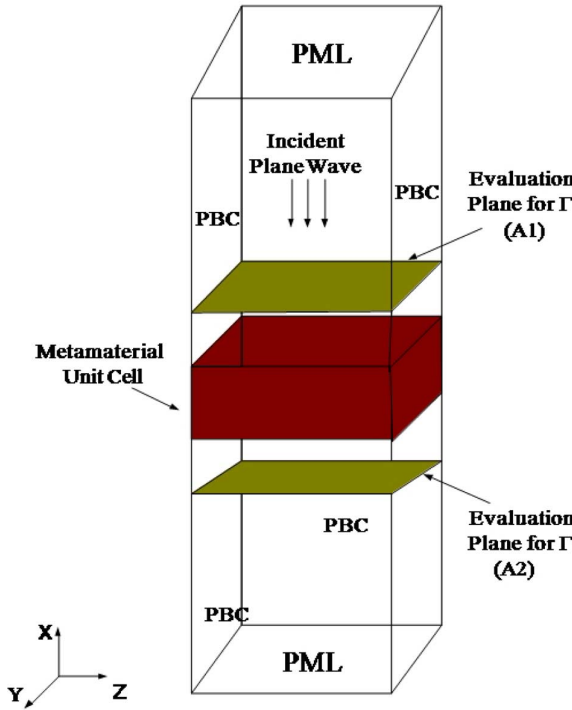


Fig. 3. Simulation setup used for numerically characterization of metamaterials.

reflection and transmission coefficients. Equations (17)–(20) give the relationship between the effective parameters and the transmission and reflection coefficients [44]–[46].

$$Z_{\text{eff}} = \pm Z_0 \sqrt{\frac{(1 + \Gamma)^2 - T^2 e^{-j2k_0 d}}{(1 - \Gamma)^2 - T^2 e^{-j2k_0 d}}} \quad (17)$$

$$e^{-jn_{\text{eff}} k_0 d} = X \pm j\sqrt{1 - X^2}, \quad (18)$$

$$X = \frac{1 - \Gamma^2 + T^2 e^{-j2k_0 d}}{2T e^{-j2k_0 d}} \quad (19)$$

$$\mu_{\text{eff}} = Z_{\text{eff}} n_{\text{eff}}, \epsilon_{\text{eff}} = \frac{n_{\text{eff}}}{z_{\text{eff}}} \quad (20)$$

where  $Z_0$  and  $k_0$  are the air characteristic impedance and wave number, respectively;  $Z_{\text{eff}}$ ,  $n_{\text{eff}}$ ,  $\epsilon_{\text{eff}}$ , and  $\mu_{\text{eff}}$  are the effective characteristic impedance, refractive index, permittivity, and permeability of the engineered material, respectively;  $\Gamma$  and  $T$  are the reflection and transmission coefficients, and  $d$  is the thickness of the engineered material. The sign in (17), and (18) is determined by the requirements that  $\text{Re}(Z_{\text{eff}}) > 0$  and  $\text{Im}(n_{\text{eff}}) < 0$  for passive media. The numerical process was carried out based on the finite element method using Ansoft HFSS10 full-wave simulation tool.

### C. The Resultant Permeability

Using the aforementioned analytical and numerical methods, the relative permeability of the proposed structures in Fig. 1 was derived and the results are shown in Figs. 4, 5. In these figures, the resultant permeability of Hilbert curve structures are compared to that of the square split spiral proposed in [17], [18]. The parameters and dimensions of all the structures are the same and are given as:  $s = w = 0.127$  mm, host dielectric of

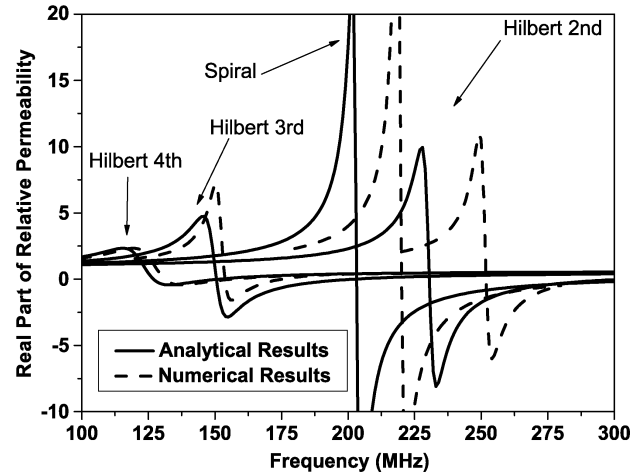


Fig. 4. Real part of resultant permeability for engineered materials with inclusions shown in Fig. 1. Analytical results (solid line) are compared with numerical results (dash line).

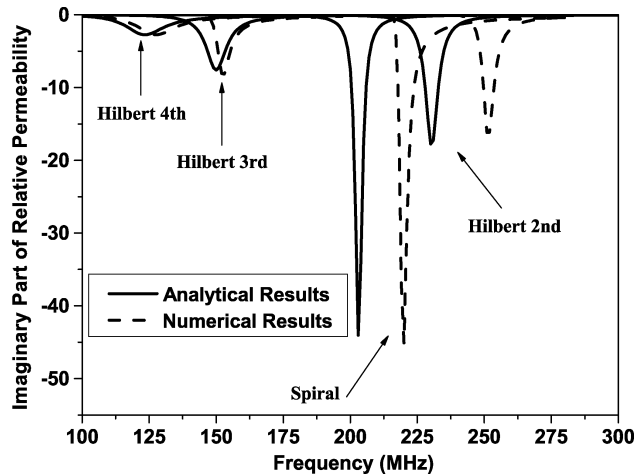


Fig. 5. Imaginary part of resultant permeability for engineered materials with inclusions shown in Fig. 1. Analytical results (solid line) are compared with numerical results (dash line).

$(\epsilon_r = 3.38, \tan \delta = 0.0027)$ ,  $l_x = 16$  mm,  $\Delta y = 3.028$  mm,  $\Delta x = \Delta z = 20$  mm, and the strips are assumed copper to model the loss.

Figs. 4 and 5 show the real and imaginary parts of the resultant permeability, computed analytically and numerically. As shown in these figures, for inclusions with 3rd or 4th order Hilbert curves, which resonate at lower frequencies, a strong agreement is observed between the analytical and numerical results. However; for the inclusions with spiral or 2nd order Hilbert curves, which resonate at higher frequencies, a frequency shift reaching a maximum value of 8.8% for the case of 2nd order Hilbert is observed between the numerical and analytical results. Since the analytical model has been derived based on the assumption of field uniformity throughout the unit cell, the smaller the inclusion in comparison to the wavelength, the more accurate the analytical model is. Therefore, the numerical simulations for inclusions based on the 3rd or 4th order Hilbert curves are expected to give closer agreement with the analytical model in comparison to inclusions based on lower order Hilbert curves.

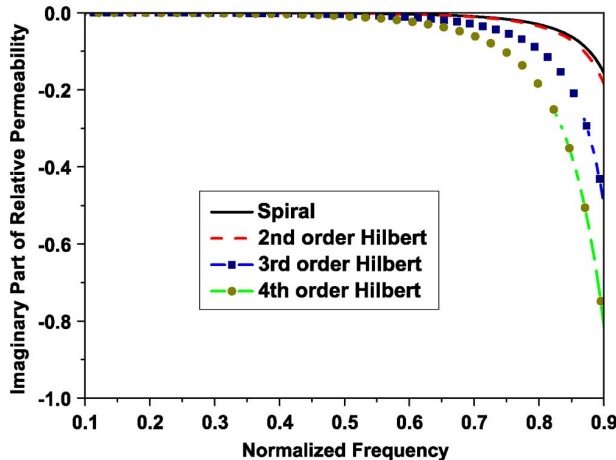


Fig. 6. Imaginary part of the resultant permeability at frequencies below the resonance. The frequency is normalized to the resonance frequency.

As shown in Fig. 4, and Fig. 5, for  $n > 2$ , fractal structures exhibit lower resonance frequency compared to the split spiral with the same size. Therefore, as predicted by the circuit model, for a given resonance frequency, using Hilbert inclusions with order of 3 or higher results in a smaller size for the unit cell compared to the split spiral. Furthermore, as shown in Fig. 4, when the order of the fractal Hilbert curve increases, the response of the permeability becomes smoother. Therefore, as predicted by the circuit model, using fractal structures decreases the rate of the permeability variation with respect to frequency leading to lower dispersion in the artificial substrate.

From Fig. 4, the maximum value achievable for the resultant permeability is smaller than that of the spiral, and this maximum value decreases as the order of Hilbert inclusions increases. This fact was also predicted by the circuit model as explained in Section II-A. In terms of loss comparison, as shown in Fig. 5, at the resonance frequency Hilbert inclusions yield lower value for the imaginary part, so they provide lower loss at the resonant frequency. Notice that it is difficult to compare the imaginary parts at the other frequencies using the scale shown in Fig. 5. For this, we have presented the imaginary part of the permeability at the frequencies below the resonance in Fig. 6. In this figure, the numerical results are used, and for the sake of comparison, the frequency is normalized to the resonance frequency for all inclusions. As shown in Fig. 6, for frequencies below resonance, the imaginary part of the permeability is higher for Hilbert inclusions than that of the spiral inclusion, and as the order of Hilbert increases the imaginary part increases. Therefore, as predicted by the circuit model, at the frequencies below the resonance Hilbert inclusions provide higher loss when compared to spirals.

### III. EXPERIMENTAL RESULTS

To verify our analytical and numerical results, an artificial magnetic material composed of 2nd order Hilbert inclusions was fabricated and characterized. A unit cell of this structure, and its dimension are shown in Fig. 7.

To measure the constitutive parameters of the artificial substrate, we use a novel microstrip-line based characterization

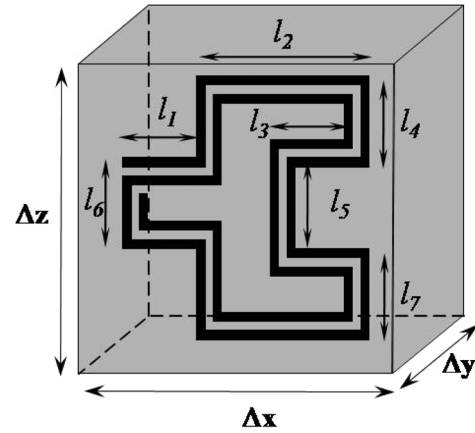


Fig. 7. One unit cell of the fabricated artificial substrate,  $s = w = 0.180 \text{ mm}$ ,  $l_1 = l_3 = l_4 = l_5 = l_6 = l_7 = 3.03 \text{ mm}$ ,  $l_2 = 6.06 \text{ mm}$ ,  $\Delta y = 3.028 \text{ mm}$ ,  $\Delta x = \Delta z = 11 \text{ mm}$ .



Fig. 8. A single strip containing 6 unit cells of inclusions fabricated using printed circuit board technology.

method reported in [40]. In this method, the permeability of the artificial substrate is extracted by measuring the input impedance of a shorted microstrip line which is implemented over the artificial substrate [40]. The advantage of this method over previously developed techniques is that the characterization can be performed by using a simple inexpensive fixture. Furthermore, no sample preparation is needed for characterization, and the same substrate designed for any microstrip device can be used for characterization as well.

Using printed circuit technology, a strip of 6 unit cells of Fractal Hilbert2 inclusions was fabricated on an FR4 substrate with  $\epsilon_r = 4.4$  and  $\tan \delta = 0.02$  (See Fig. 8). Forty of these strips were then stacked in the  $y$  direction to provide a three-dimensional substrate. Due to the thickness of the metal inclusions, an average air gap of  $50 \mu\text{m}$  develops between the strips in the stacking process. The air space, while unavoidable in the fabrication process, is nevertheless measurable so it can be easily included in the design.

#### A. Permittivity Measurement

Using the engineered substrate and two conducting plates, a parallel-plate metamaterial capacitor was fabricated, and by measuring its capacitance, the permittivity of the artificial substrate was calculated [18].

According to the classical image theory, using only one period of the artificial unit cells, in the area between the two metallic parallel plates, can mimic the behavior of an infinite array of unit cells, which is the default assumption in the analysis and design of artificial structures. This property, therefore, makes the method presented in [18] highly robust and well-suited for metamaterial characterization. It is interesting

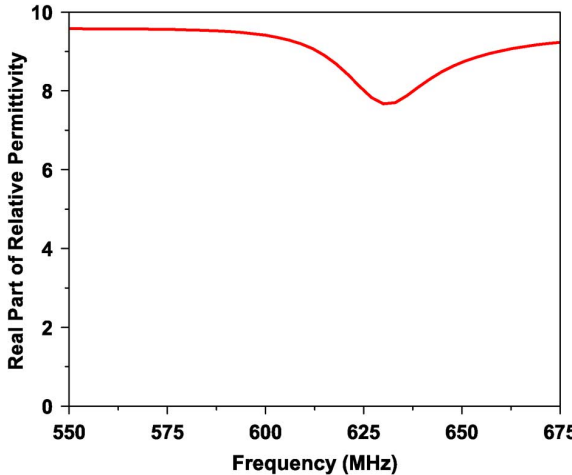


Fig. 9. Simulation results for extracted permittivity (real part).

to note, however, that the authors of [18] observed a rather large difference between the analytically estimated and measured permittivity values (a difference of more than 30%). The large discrepancy is in fact due to the approximations used in the derivation of the analytical formula. For the same artificial structure measured in [18], we have performed a full wave numerical simulation using the simulation setup discussed in Section II-B and obtained a difference between simulation and measurements of less than 7%.

Using the aforementioned method, the x-directed permittivity for this artificial magnetic substrate was measured, at the low frequency of 10 MHz, as  $\epsilon_x = 9.60$  [40]. By using the simulation setup explained in Section II and Ansoft HFSS10, the permittivity of the artificial magnetic substrate was numerically calculated as  $\epsilon_x = 9.58$ , thus showing good agreement with measurement. In the simulation, the  $50 \mu\text{m}$  air gap was included. However; the simulation results show that the resultant permittivity changes with frequency in such a way that at the resonance frequency of 630 MHz, the permittivity decreases to 7.6 (see Fig. 9). The method used in [40] is not suitable to measure the permittivity as a function of frequency; however, since the measurement results at low frequency are close to the simulation result, the subsequent calculation of the permeability is expected to yield a comparable level of accuracy.

### B. Permeability Measurement

The same substrate that is used for permittivity measurement is used as a substrate of the shorted microstrip line to extract the permeability. The fabricated fixture used for permeability measurement is shown in Fig. 10. The fabricated substrate has dimensions of 12, 8.2, and 1.1 cm in the y, z, and x directions, respectively. For the quasi-TEM dominant mode, the  $\mathbf{H}$  and  $\mathbf{E}$  fields in the substrate will be in the y and x directions, respectively. Therefore this configuration can be used for retrieval of  $\mu_y$ .

Using a vector network analyzer, the complex input impedance of the shorted microstrip line shown in Fig. 10 is measured over the frequency range of 500–680 MHz. Then using the data shown in Fig. 9 for  $\epsilon_x$  and measured impedance,  $\mu_y$  is extracted by the method reported in [40]. The real and

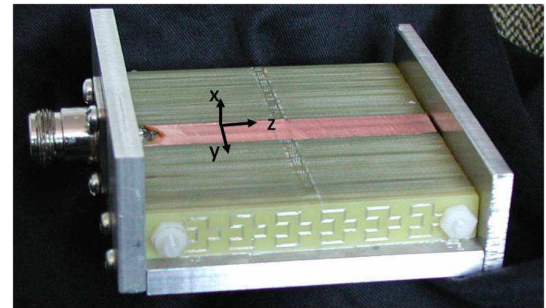


Fig. 10. The fabricated fixture used for permeability measurement.

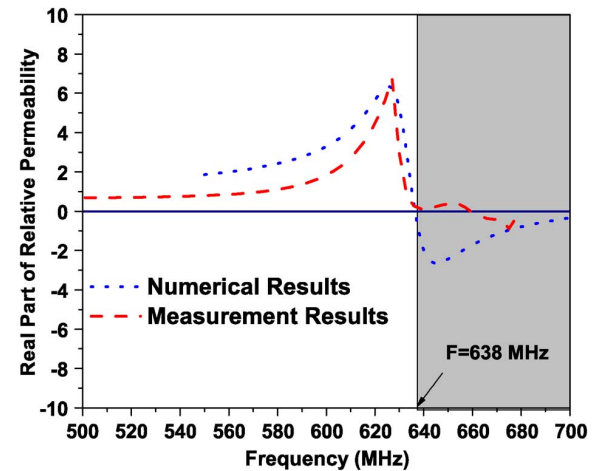


Fig. 11. The measured and numerically simulated real part of the permeability for the artificial magnetic material shown in Fig. 10.

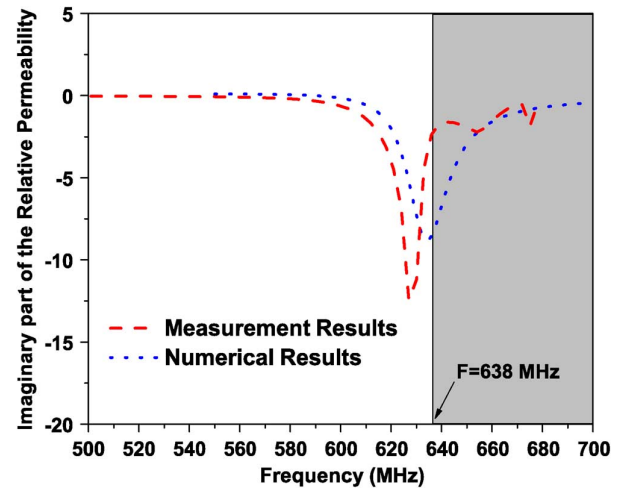


Fig. 12. The measured and numerically simulated imaginary part of the permeability for the artificial magnetic material shown in Fig. 10.

imaginary parts of the measured y-directed permeability are shown in Fig. 11 and Fig. 12. The measurement data shown in these figures are from [40]. In these figures, the measurement results are compared with the numerical simulation results. The  $50 \mu\text{m}$  air gap was also included in the simulation. Unfortunately this air gap cannot be modeled within the analytical formulas presented in Section II. The analytical model, which does not consider the air gap, results in a resonant frequency

of 520 MHz, corresponding to a 16% shift when compared to the simulation results that included the air gap. A similar shift in the resonance frequency due to the air gap has also been reported in previous works [18].

The shaded area in Fig. 11 and Fig. 12 determines the frequencies over which the real part of the permeability is negative. As explained in [40], over this frequency range corresponding to frequencies higher than 638 MHz, the measurement results are not valid due to the restriction of the formulas used for microstrip effective permeability in [40]. As explained in [40], the formulas exist in literature for microstrip effective permeability are derived using conformal mapping technique where the permeability was assumed positive. Therefore, these equations cannot be used at over the frequency range where the permeability is negative. However, since artificial magnetic materials are designed to operate at frequencies over which the permeability is positive, characterization of the permeability behavior at those frequencies would be sufficient for application purposes. Over the frequency range where the real part of the permeability is positive, good agreement is observed between the simulation and measurement results.

As briefly discussed above and more extensively in [40], in the numerical analysis, periodic boundary conditions are used to mimic an infinite number of unit cells. However, in practice we can only realize a finite number of unit cells. For example in the setup used in this work (see Fig. 10), the fabricated substrate contains 6 unit cells of inclusions in the z direction and only one unit cell in the x direction. Therefore; we do not expect a very strong agreement between simulation and measurements. By analyzing the induced magnetic field distribution within the inclusion, we observed that at the resonance frequency, a strong magnetic field is present mainly at the center of the inclusion. However, at frequencies below resonance, we observe a relatively weak field at the sides of the inclusion (the sides normal to the x-direction in Fig. 9). Accordingly, at the resonance frequency the adjacent unit cells in the x direction have a minor effect on the resultant permeability, while at the frequencies below resonance, this effect is not negligible. This observation could potentially explain the fact that we have good agreement between simulation and measurement at the resonance frequency, but the agreement becomes weaker for frequencies below resonance (see Fig. 11).

It is most likely that increasing the number of unit cells in the x-direction provides higher homogeneity in the fabricated substrate which will result in a better agreement between numerical and measurement results. On the other hand, in a wide class of applications such as antenna miniaturization, only one unit cell is used in the x direction [21]–[24], and therefore, the measurement results would be of strong relevance.

#### IV. CONCLUSIONS

The use of Fractal curves to miniaturize artificial magnetic materials was investigated. Novel configurations were proposed to realize artificial magnetic materials with smaller unit cells by combining the square split loop configuration with Fractal Hilbert curves. The new designs are desirable when designing low profile miniaturized antennas in which the engineered magnetic materials are used as the substrate. Analytical models were

introduced to design and analyze the new structures. The analytical model was validated through both full wave simulation and experimental characterization. It was shown that using forth order of Fractal Hilbert curve, it is possible to realize inclusions as small as 0.014 of the wavelength in the dielectric. This size is 63% of the size of spiral inclusion and 32% of the size of SRR. Using higher order Hilbert curves results in even further miniaturization of the unit cell. In terms of the electromagnetic properties, the new structures provide lower frequency dispersion and lower magnetic loss at the resonance frequency in comparison to the simple square spiral inclusions. This advantage comes at the expense of lower permeability and higher magnetic loss at frequencies below resonance.

#### REFERENCES

- [1] R. C. Hansen and M. Burke, "Antennas with magneto-dielectrics," *Microw. Opt. Tech. Lett.*, vol. 26, no. 2, pp. 75–78, Jun. 2000.
- [2] A. Buerkle and K. Sarabandi, "A circularly polarized magneto-dielectric resonator antenna with wideband, multi-resonant response," in *Proc. IEEE AP-S Int. Symp. Antennas Propag.*, Jul. 2005, vol. 1B, pp. 487–490.
- [3] K. Min, T. V. Hong, and D. Kim, "A design of a meander line antenna using magneto-dielectric material for RFID system," in *Proc. Asia-Pacific Conf. on Microwave*, Dec. 2005, vol. 4, pp. 1–4.
- [4] A. Foroozesh and L. Shafai, "Size reduction of a microstrip antenna with dielectric superstrate using meta-materials: Artificial magnetic conductors versus magneto-dielectrics," in *Proc. IEEE AP-S Int. Symp. Antennas Propag.*, July 2006, vol. 1B, pp. 11–14.
- [5] L. Yousefi and O. Ramahi, "Engineered magnetic materials with improved dispersion using multi-resonator structures," in *Proc. Canadian Conf. on Electrical and Computer Engineering*, Apr. 2007, pp. 966–969.
- [6] L. Yousefi and O. Ramahi, "Miniaturized wideband antenna using engineered magnetic materials with multi-resonator inclusions," in *Proc. IEEE Antennas and Propagation Society Int. Symp.*, Jun. 2007, pp. 1885–1888.
- [7] L. Yousefi, B. Mohajer-Iravani, and O. M. Ramahi, "Enhanced bandwidth artificial magnetic ground plane for low profile antennas," *IEEE Antenna Wireless Propag. Lett.*, vol. 6, pp. 289–292, Jun. 2007.
- [8] H. Mosallaei and K. Sarabandi, "Magneto-dielectrics in electromagnetics: Concept and applications," *IEEE Trans. Antennas Propag.*, vol. 52, no. 6, pp. 1558–1567, Jun. 2004.
- [9] K. N. Rozanova, Z. W. Li, L. F. Chen, and M. Y. Koledintseva, "Microwave permeability of co<sub>2</sub>Z composites," *J. Appl. Phys.*, vol. 97, pp. 013 905-1–013 905-7, Dec. 2004.
- [10] A. L. Adenot, O. Acher, T. Taffary, and L. Longuet, "Sum rules on the dynamic permeability of hexagonal ferrites," *J. Appl. Phys.*, vol. 91, pp. 7601–7603, May 2002.
- [11] O. Acher and A. L. Adenot, "Bounds on the dynamic properties of magnetic materials," *Phys. Rev. B*, vol. 62, no. 17, pp. 11 324–11 327, Nov. 2000.
- [12] W. D. Callister, *Materials Science and Engineering, an Introduction*. New York: Wiley, 2000.
- [13] M. V. Kostin and V. V. Shevchenko, "Artificial magnetics based on double circular elements," in *Proc. Bian-Isotropics'94*, Périgueux, May 1994, pp. 49–56.
- [14] J. B. Pendry, A. J. Holden, D. J. Robbins, and W. J. Stewart, "Magnetism from conductors and enhanced nonlinear phenomena," *IEEE Trans. Microw. Theory Tech.*, vol. 47, no. 11, pp. 2075–2084, Nov. 1999.
- [15] R. Marqués, F. Medina, and R. Rafii-El-Idrissi, "Role of bianisotropy in negative permeability and left-handed metamaterials," *Phys. Rev. B*, vol. 65, no. 14, pp. 44 401–44 405, Apr. 2002.
- [16] S. Maslovski, P. Ikonen, I. Kolmakov, and S. Tretyakov, "Artificial magnetic materials based on the new magnetic particle: Metasolenoid," *Progr. Electromagn. Res. (PIER)*, vol. 54, no. 9, pp. 61–81, Sept. 2005.
- [17] J. D. Baena, R. Marques, F. Medina, and J. Martel, "Artificial magnetic metamaterial design by using spiral resonators," *Phys. Rev. B*, vol. 69, pp. 144 021–144 025, Jan. 2004.
- [18] K. Buell, H. Mosallaei, and K. Sarabandi, "A substrate for small patch antennas providing tunable miniaturization factors," *IEEE Trans. Microw. Theory Tech.*, vol. 54, pp. 135–146, Jan. 2006.

- [19] P. M. T. Ikonen, S. I. Maslovski, C. R. Simovski, and S. A. Tretyakov, "On artificial magnetodielectric loading for improving the impedance bandwidth properties of microstrip antennas," *IEEE Trans. Antennas Propag.*, vol. 54, no. 6, pp. 1654–1662, Jun. 2006.
- [20] S. A. Schelkunoff and H. T. Friis, *Antennas: Theory and Practise*. New York: Wiley, 1952.
- [21] M. K. Karkkainen, S. A. Tretyakov, and P. Ikonen, "Numerical study of PIFA with dispersive material fillings," *Microw. Opt. Tech. Lett.*, vol. 45, no. 1, pp. 5–8, Feb. 2005.
- [22] M. E. Ermutlu, C. R. Simovski, M. K. Karkkainen, P. Ikonen, S. A. Tretyakov, and A. A. Sochava, "Miniaturization of patch antennas with new artificial magnetic layers," in *Proc. IEEE Int. Workshop on Antenna Technology*, Mar. 2005, vol. 1B, pp. 87–90.
- [23] P. Ikonen, S. Maslovski, and S. Tretyakov, "Pifa loaded with artificial magnetic material: Practical example for two utilization strategies," *Microw. Opt. Tech. Lett.*, vol. 46, no. 3, pp. 205–210, Jun. 2005.
- [24] M. K. Karkkainen and P. Ikonen, "Patch antenna with stacked split-ring resonators as artificial magnetodielectric substrate," *Microw. Opt. Tech. Lett.*, vol. 46, no. 6, pp. 554–556, Jul. 2005.
- [25] H. Mosallaei and K. Sarabandi, "Design and modeling of patch antenna printed on magneto-dielectric embedded-circuit metasubstrate," *IEEE Trans. Antennas Propag.*, vol. 55, pp. 45–52, Jan. 2007.
- [26] P. M. T. Ikonen and S. A. Tretyakov, "Comments on "Design and modeling of patch antenna printed on magneto-dielectric embedded-circuit metasubstrate"," *IEEE Trans. Antennas Propag.*, vol. 55, pp. 2935–2936, Oct. 2007.
- [27] H. Mosallaei and K. Sarabandi, "Reply to comments on 'design and modeling of patch antenna printed on magneto-dielectric embedded-circuit metasubstrate,'" *IEEE Trans. Antennas Propag.*, vol. 55, pp. 2936–2937, Oct. 2007.
- [28] A. Erentok, R. W. Ziolkowski, J. A. Nielsen, R. B. Greegor, C. G. Parazzoli, M. H. Tanielian, S. A. Cummer, B.-I. Popa, T. Hand, D. C. Vier, and S. Schultz, "Low frequency lumped element-based negative index metamaterial," *Appl. Phys. Lett.*, vol. 91, pp. 1 841 041–1 841 043, Nov. 2007.
- [29] E. A. Parker and A. N. A. E. Sheikh, "Convolved array elements and reduced size unit cells for frequency-selective surfaces," in *Proc. Inst. Electr. Eng. Microw. Antennas, Propag.*, 1991, vol. 138, pp. 19–22.
- [30] J. McVay, N. Engheta, and A. Hoofar, "High-impedance metamaterial surfaces using hilbert-curve inclusions," *IEEE Microw. Wireless Comp. Lett.*, vol. 14, pp. 130–132, Mar. 2004.
- [31] J. McVay, A. Hoofar, and N. Engheta, "Peano high-impedance surfaces," in *Proc. Radio Sci.*, 2005, vol. 40.
- [32] L. Zhou, W. Wen, C. T. Chan, and P. Sheng, "Multiband subwavelength magnetic reflectors based on fractals," *Appl. Phys. Lett.*, vol. 83, no. 16, pp. 3257–3259, 2003.
- [33] W. Zhang, A. Potts, D. Bagnall, and B. Davidson, "High-resolution electron beam lithography for the fabrication of high-density dielectric metamaterials," *J. Thin Solid Films*, vol. 515, no. 7–8, pp. 3714–3717, 2007.
- [34] A. Mejdoubi and C. Brosseau, "Intrinsic resonant behavior of metamaterials by finite element calculations," *Phys. Rev. B*, vol. 74, no. 16, p. 165424, 2006.
- [35] J. McVay, A. Hoofar, and N. Engheta, "Bandwidth enhancement and polarization dependence elimination of space-filling curve artificial magnetic conductors," in *Proc. Asia-Pacific Microwave Conf.*, Dec. 2007, pp. 1–4.
- [36] J. McVay, N. Engheta, and A. Hoofar, "Numerical study and parameter estimation for double-negative metamaterials with Hilbert-curve inclusions," in *Proc. IEEE AP-S Int. Symp. Antennas Propag.*, Jul. 2005, vol. 2B, pp. 328–331.
- [37] V. Crnojevic-Bengin, V. Radonic, and B. Jokanovic, "Fractal geometries of complementary split-ring resonators," *IEEE Trans. Microw. Theory Tech.*, vol. 56, no. 10, pp. 2312–2321, Oct. 2008.
- [38] V. Pierro, J. McVay, V. Galdi, A. Hoofar, N. Engheta, and I. M. Pinto, "Metamaterial inclusions based on grid-graph Hamiltonian paths," *Microw. Opt. Tech. Lett.*, vol. 48, no. 12, pp. 2520–2524, Dec. 2006.
- [39] L. Yousefi and O. M. Ramahi, "New artificial magnetic materials based on fractal Hilbert curves," in *Proc. IWAT07*, Mar. 2007, pp. 237–240.
- [40] L. Yousefi, H. Attia, and O. M. Ramahi, "Broadband experimental characterization of artificial magnetic materials based on a microstrip line method," *J. Progr. Electromagn. Res. (PIER)*, vol. 90, pp. 1–13, Feb. 2009.
- [41] J. Franklin and A. Daoud, *Proof in Mathematics: An Introduction*. New York: Quakers Hill Press, 1996.
- [42] R. Schinzinger and P. A. A. Laura, *A Conformal Mapping: Methods and Applications*. The Netherlands: Elsevier, 1991.
- [43] K. E. Oughstun and N. A. Cartwright, "On the Lorentz-Lorenz formula and the Lorentz model of dielectric dispersion," *Opt. Expr.*, vol. 11, no. 13, pp. 1541–1546, Jun. 2003.
- [44] X. Chen, T. M. Grzegorczyk, B. Wu, J. Pacheco, and J. A. Kong, "Robust method to retrieve the constitutive effective parameters of metamaterials," *Phys. Rev. E*, vol. 70, no. 1, pp. 016 608.1–016 608.7, Jul. 2004.
- [45] K. Buell and K. Sarabandi, "A method for characterizing complex permittivity and permeability of metamaterials," in *Proc. IEEE AP-S Int. Symp. Antennas Propag.*, Jun. 2002, vol. 2, pp. 408–411.
- [46] R. W. Ziolkowski, "Design, fabrication, and testing of double negative metamaterials," *IEEE Trans. Antennas Propag.*, vol. 51, no. 7, pp. 1516–1529, Jul. 2003.



**Leila Yousefi** (M'09) was born in Isfahan, Iran, in 1978. She received the B.Sc. and M.Sc. degrees in electrical engineering from Sharif University of Technology, Tehran, Iran, in 2000 and 2003, respectively, and the Ph.D. degree in electrical engineering from the University of Waterloo, Waterloo, ON, Canada, in 2009.

Currently she is working as a Postdoctoral Fellow at the University of Waterloo. Her research interests include metamaterials, miniaturized antennas, electromagnetic bandgap structures, and MIMO systems.



**Omar M. Ramahi** (F'09) received the B.S. degrees in mathematics and electrical and computer engineering (*summa cum laude*) from Oregon State University, Corvallis, and the M.S. and Ph.D. degrees in electrical and computer engineering from the University of Illinois at Urbana-Champaign.

From 1990–to 993, he held a visiting fellowship position at the University of Illinois at Urbana-Champaign. From 1993 to 2000, he worked at Digital Equipment Corporation (presently, HP), where he was a member of the alpha server product development group. In 2000, he joined the faculty of the James Clark School of Engineering, University of Maryland at College Park, first as an Assistant Professor, later as a tenured Associate Professor, and where he was also a faculty member of the CALCE Electronic Products and Systems Center. Presently, he is a Professor in the Electrical and Computer Engineering Department and holds the NSERC/RIM Industrial Research Associate Chair, University of Waterloo, ON, Canada. He holds cross appointments with the Department of Mechanical and Mechatronics Engineering and the Department of Physics and Astronomy. Previously, he served as a consultant to several companies and was a co-founder of EMS-PLUS, LLC and Applied Electromagnetic Technology, LLC. He has authored and coauthored over 240 journal and conference papers. He is a coauthor of the book *EMI/EMC Computational Modeling Handbook* (Springer-Verlag, 2001).

Prof. Ramahi serves as an Associate Editor for the IEEE TRANSACTIONS ON ADVANCED PACKAGING and as the IEEE EMC Society Distinguished Lecturer.